Supporting Information

Exchange-Coupled Bimagnetic Cobalt/Iron Oxide Branched Nanocrystal Heterostructures

*Marianna Casavola,[1,2] Andrea Falqui,[3] Miguel Angel Garcia,[4,5] Mar García-Hernández,[6] Cinzia Giannini,[7] Roberto Cingolani[2,3] P. Davide Cozzoli[1,2]**

[1]Scuola Superiore ISUFI, University of Salento, Distretto Tecnologico ISUFI, 73100 Lecce, Italy
[2]National Nanotechnology Laboratory of CNR-INFM, Unità di Ricerca IIT, via per Arnesano km 5, I-73100 Lecce, Italy;
[3] Istituto Italiano di Tecnologia, IIT, via Morego 30, I-16163 Genova, Italy
[4] Department of Material Physics, University Complutense, E-28024 Madrid, Spain
[5] Instituto de Ceramica y Vidrio, CSIC, C/ Kelsen 5, Campus de Cantoblanco, E-28049 Madrid , Spain
[6] Instituto de Ciencia de Materiales de Madrid, CSIC, C/ Sor Juana Ines de la Cruz 3, Campus de Cantoblanco, E-28049 Madrid , Spain
[7] Istituto di Cristallografia (IC-CNR), via Amendola 122/O, I-70126 Bari, Italy

* To whom all correspondence should be addressed: Phone:+39 0832 298231 Fax: +39 0832 298230 E-mail: davide.cozzoli@unile.it

1. Experimental Details

Materials. All chemicals were of the highest purity available and were used as received. Oleic acid ($C_{17}H_{33}CO_2H$ or OLAC, 90%), oleyl amine ($C_{17}H_{33}NH_2$ or OLAM, 70%), 1-octadecene ($C_{18}H_{36}$ or ODE, 90%), iron pentacarbonyl ($Fe(CO)_5$, 98%), and dodecan-1,2-diol ($C_{12}H_{24}(OH)_2$ or DDIOL, 90%) and purchased from Aldrich. Dicobalt octacarbonyl ($Co_2(CO)_8$, stabilized with 1-5% of hexane) was purchased from Strem. All solvents were purchased from Aldrich. The Fe and Co standards for ICP-AES analyses were from Romil.

Synthesis procedures All the synthesis procedures were carried out under nitrogen atmosphere, using a standard Schlenk line set-up.

Iron oxide nanocrystal tetrapods (TPs) with varying geometric parameters, henceforth referred to as the "seeds", were synthesized by a literature procedure, which involved thermal decomposition of $Fe(CO)_5$ at 240-280 °C in a ternary surfactant mixture composed of DDIOL:OLAC:OLAM at a 5:3:3 molar ratio in ODE, followed by mild oxidation under air at 80°C.[1] A stock seed solution was prepared under ambient conditions by dissolving the appropriate amounts of purified TPs in toluene so as to realize a concentration of 0.5 M (expressed in Fe units according to ICP-AES measurements).

In a typical synthesis of Co/iron oxide HNCs, 0.5-2 mL of the TP seed stock solution was mixed with 5 mL of ODE in a 50 mL three-neck flask connected to a reflux cooler and degassed at 120° for 30 min to remove toluene and oxygen residuals. The system was then purged with nitrogen and heated up to 180° C under inert flow. At this point, 0.5-2 mL of a 0.2 M cobalt precursor solution (prepared by dissolving the appropriate amount of $Co_2(CO)_8$ in previously degassed ODE in a glove box) was injected drop-wise into the seed containing solution at a rate of 0.1 ml/min by means of a syringe pump (GENIE Plus Syringe Pump, Kent Scientific). After the injection, the precursor decomposition was allowed to proceed to completion in an additional 20 min, after which 1 mmol of previously degassed OLAC was quickly added to the mixture in a single portion. The flask was kept at 180° for an additional 10 min to ensure surfactant stabilization of the HNCs, after which the reaction was halted by removing the heating mantle. The flask was cooled down to room temperature and transferred to a glove box. The TPs were precipitated from their reaction mixture upon addition of anhydrous 2-propanol, separated by centrifugation, and thoroughly washed with 2-propanol. The final HNCs were dissolved in anhydrous toluene and stored under nitrogen.

For comparison purposes, samples of Co NCs were synthesized by a procedure similar to the one used for HNC synthesis in the complete absence of TP seeds. Such NCs were found to be characterized by polycrystallinity as well as by crystal-phase composition similar to the one assessed for Co domains heterogeneously nucleated on TPs seeds.

Transmission Electron Microscopy (TEM) Low-magnification TEM images were recorded with a Jeol Jem 1011 microscope operating at an accelerating voltage of 100 kV. Statistical size determinations were performed by examining 200 particles in low magnification TEM images with a dedicated software (Axio Vision). Phase-contrast high-resolution TEM (HRTEM) measurements were performed with a Jeol 2100F microscope working at an accelerating voltage of 200 kV. The microscope was equipped with a field emission gun for scanning transmission electron microscopy (STEM) imaging mode. Energy-dispersive X-ray (EDX) spectra were acquired with a Bruker spectrometer by scanning an electron probe size of 1 nm on the nanocrystals. The samples were prepared in a glove box by depositing a few drops of a dilute HNC solution onto carbon-coated copper grids, which were immediately transferred to the microscope.

Elemental Analysis The Fe and Co atomic content of nanocrystal samples was measured by inductively coupled plasma atomic emission spectroscopy (ICP-AES) measurements with a Varian Vista AX spectrometer. The samples for analyses were digested in concentrated HCl/HNO_3 (3/1 v/v)

Powder X-ray Diffraction (XRD). XRD measurements were performed with a NONIUS KappaCCD single-crystal diffractometer equipped with a 3 kW generator molybdenum tube, with a high-precision four-circle goniometer, and a low-noise and high-sensitivity CCD detector. The dried sample powders, loaded into Lindemann capillaries (0.5 mm diameter) under the inert atmosphere of a glove box, were measured in Debye-Scherrer configuration. The images were folded into powder diffraction patterns using the FIT2D software[2] after calibrating the detector with Si-NIST (640c) powder standard. Due to the instrumental resolution function, crystalline domains larger than ~4 nm could not be discriminated by their XRD peak broadening.

Quantitative phase analysis (QPA) of XRD patterns was performed with a whole profile pattern fitting program *Quanto* based on the Rietveld method.[3] The sample was described as a mixture of different crystal-phases of Co and iron oxide. Consequently, the whole diffraction pattern was given by the sum of the background level and the Bragg diffracted intensity, of each crystalline phase, weighted according to phase weight fractions derived from refined scale parameters. The peak intensity was computed by the crystal structure model (chemical species and atomic position in the unit cell).

The crystallographic data used in the analysis were: a unit cell size of 8.268 Å and a *F d -3 m* space group for the magnetite; a unit cell size of 8.3457 Å and a *P* 4_3 *3 2* space group for the maghemite; a unit cell of 6.1154 Å and a *P* 4_1 *3 2* space group for the epsilon Co phase (*ε-Co*); cell parameters a=b=2.506 Å and c=4.069 Å and a *P* 6_3*/m m c* space group for the hexagonal close packed Co phase (*hcp-Co*). The peak shape and width were described by a Pearson VII analytical

function with adjustable parameters. The background is described by a Young polynomial with refinable coefficients. The accuracy of the weight fraction evaluation was estimated by a Goodness of Fit statistical indicator (GoF), which takes the value of 1 for an ideal fit. GoF values of <3-4 were considered satisfactory. The error in the calculated phase fraction value was around 2-4%.

Magnetic Measurements Magnetic measurements were performed on dried nanocrystal powder samples using a MPMS Quantum Design SQUID magnetometer. All the powder samples were prepared in a glove-box at room temperature, as described for the XRD measurements, and then measured under inert atmosphere. The samples corresponding to TP-Co physical mixtures (referred to as MIX in the main manuscript) were prepared by co-mixing appropriate volumes of deaerated solutions of purified iron oxide TPs and separately synthesized Co NCs, and inducing their co-precipitation upon alcohol addition.

Samples were always handled with plastic tools and gloves to avoid any possible contamination with metallic particles. For each sample, a new sample holder was used. The effect of sample oxidation on the magnetic properties was assessed by measuring the powders after air exposure under ambient conditions for 30 days, after which a stable oxidation layer on the Co domain was obtained

2. Size-selective precipitation of HNCs

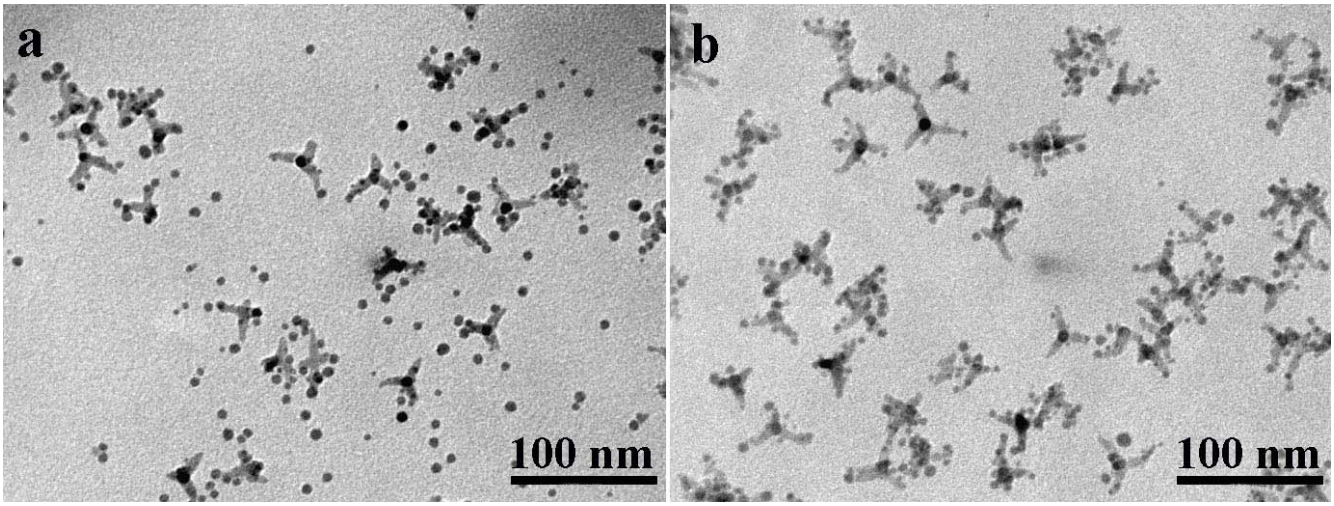

Figure S1 Example of size-selective precipitation applied to mixtures of HNCs and separately nucleated Co NCs, which were prepared at exceedingly high Co:Fe molar ratios: (**a**) the starting nanocrystal product; (**b**) Co-decorated TPs size-sorted by calibrated 2-propanol addition to chloroform solution of the nanostructures, followed by centrifugation and redissolution.

3. Quantitative phase analysis (QPA) of XRD data

We evaluated the crystal-phase composition of the samples by fitting the experimental XRD data with a whole profile pattern fitting program *Quanto* based on the Rietveld method. As a representative example of the outcome of this procedure, the experimental XRD pattern of Co-decorated tetrapod HNCs is examined in **Fig. S2**. The sample was supposed to be a three-phase mixture made of ε-Co, hcp-Co and inverse spinel cubic iron oxide. Fig. S1 shows that a satisfactory fit could be obtained, with the corresponding GoF index being lower than 3. Although minor amounts of other phases could not be ruled out completely, the high fit quality and the GoF index values indeed proved that the initial assumption was reliable.

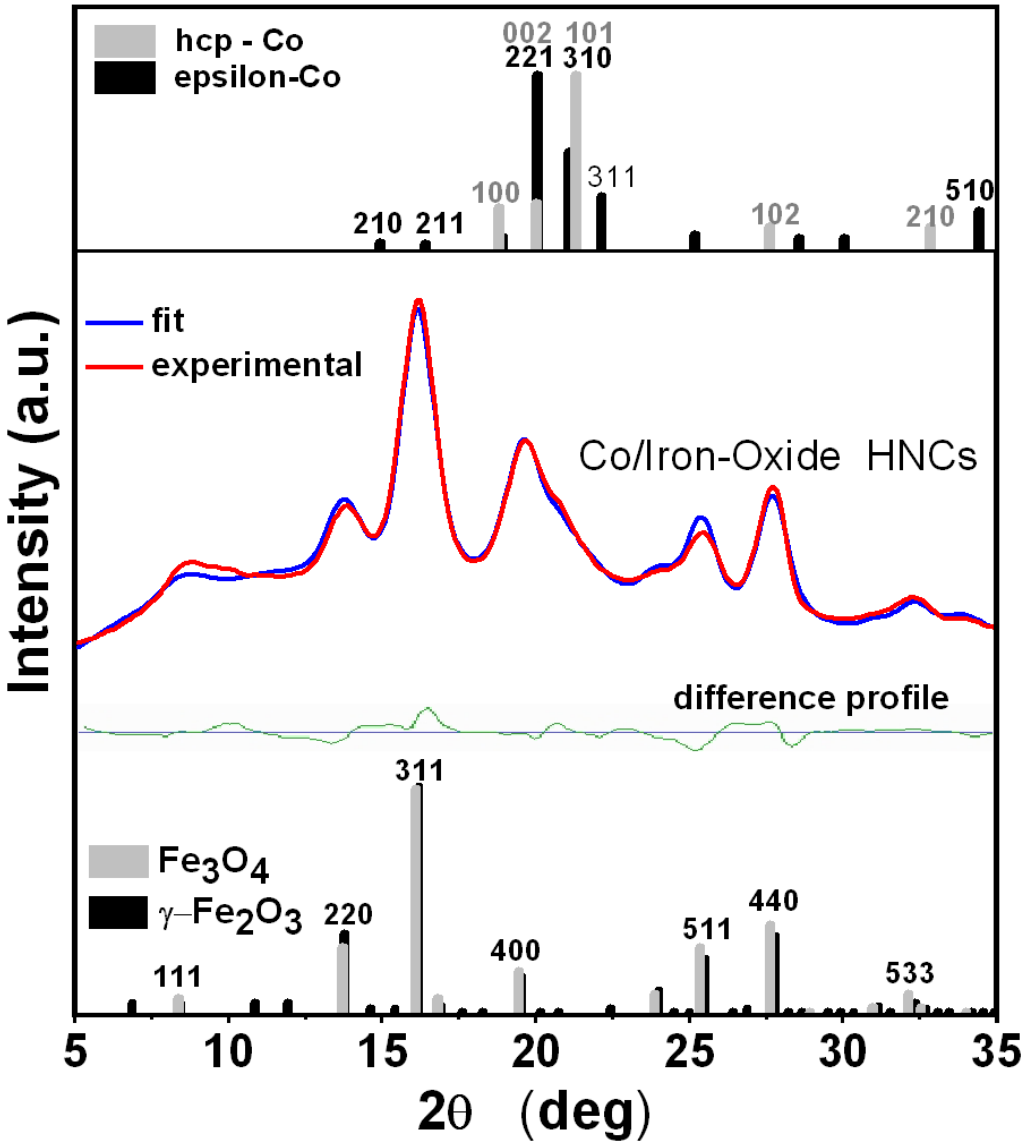

Figure S2 Comparison between the experimental XRD pattern of Co-decorated tetrapods and the QPA fitting (which corresponds to samples in Fig. 2 in the manuscript). The difference profile between experimental and calculated curves is also shown. The crystal-phase composition of the sample was found to be: *ε*-Co ~5%; *hcp*-Co ~20%; and iron oxide ~75%.

4. Additional STEM-EDX analyses

Depending on the orientation of the HNCs on the TEM grid, detection of substantially intense signals of both Co K_α and Fe K_α from locations that are instead expected to exhibit a majority of either Fe K_α (e.g. the TP arms) or Co K_α counts (e.g., the clearly spherical domains), respectively, could reasonably be due to acquisition of X-ray fluorescence from regions where the Co and the iron oxide domains partially superimpose with each other. An example is shown in **Fig. S3**.

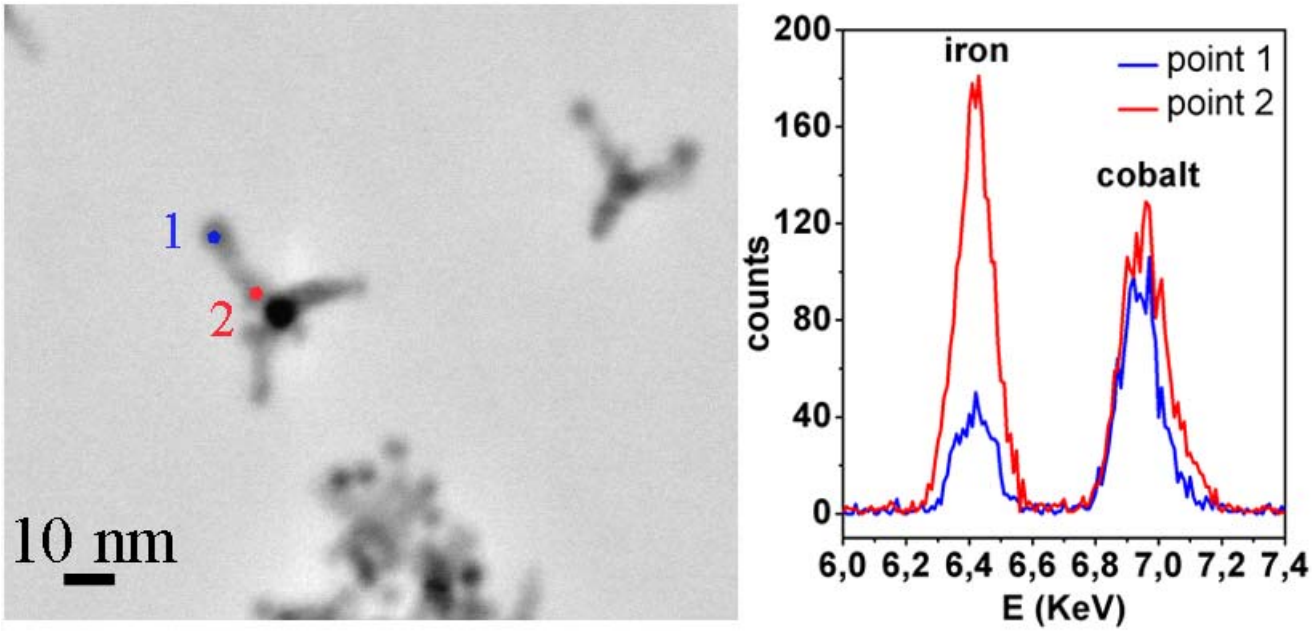

Figure S3: STEM image of an individual HNC (left panel) where the coloured spots indicate the points from which the corresponding EDX spectra (right panel) were recorded. In correspondence of points "1" where the visible tetrapod arm appears to terminate with one spherical domain (left panel), the Co K_α contribution is clearly dominant over that from Fe K_α (right panel, blue trace); differently, at point "2" where one spherical domain can be observed to overlap with the tetrapod arm (left panel), the counts of Fe K_α and Co K_α are both relevant (right panel, red trace).

5. Monitoring of HNC growth

The temporal evolution of HNC growth was monitored by withdrawing aliquots of the hot reaction mixture via a glass syringe at scheduled time intervals. The aliquots were suddenly cooled down to room temperature and transferred into a glove box for extraction and purification. A typical time sequence of HNC formation is shown in **Fig. S4**. The observed evolution of the HNC topology and dimensions indicated that heterostructure formation proceeded via direct heterogeneous nucleation of Co "patches" onto the iron oxide TP seeds, followed by the gradual enlargement of these domains over time. This mechanism was supported by the following observations:

(i) In the hypothesis of aggregation-based growth pathways, an initial nucleation and growth of separate Co NCs should be observed, which should then attach permanently the TPs. If such a mechanism were operative, one should detect the progressive increase in the population of HNCs at the expense of the population of both the TPs and of homogeneously nucleated Co NCs. However, such a growth sequence was never observed, whereas the relative fraction of the HNCs relative to that of separated Co NCs (whenever present) kept constant over time.

(ii) The exclusive formation of a particular type of HNC topology (i.e., Co-decorated TPs) allowed us to discredit further any aggregation-based growth mechanism, as the latter should in fact lead also to detection of other types of particle oligomers incorporating TPs and/or Co NPs in variable numbers.

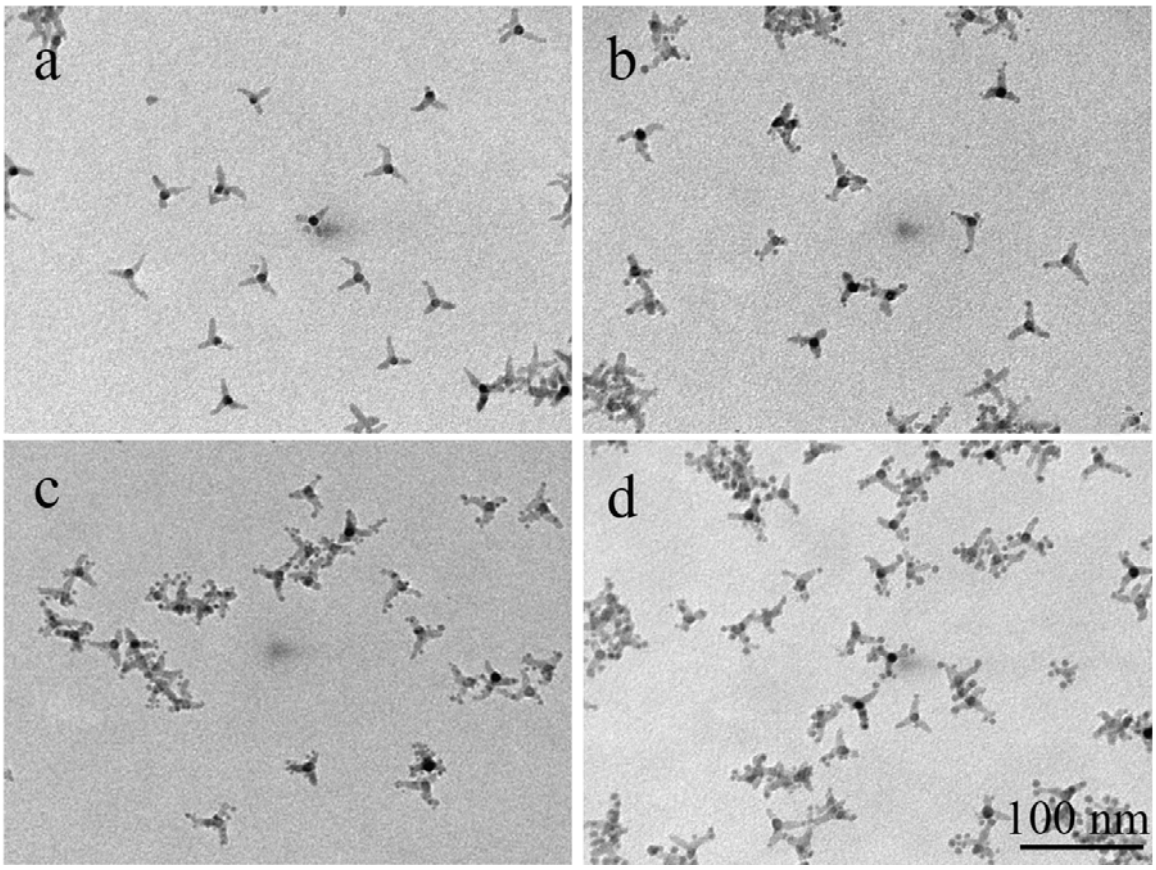

Figure S4 Typical evolution of HNC formation at different reaction times: (a) 0 min; (b) 10 min; (c) 15 min; (d) 20 min. The required $Co_2(CO)_8$ precursor amount was diluted with 2.5 g of ODE and added by means of a syringe pump over a time period of 20 min. The initial iron oxide seed concentration (expressed in Fe units) was 0.04 M, while the Co:Fe reactant molar ratio was set at 0.6.

6. Control synthesis experiments: role of surfactants in HNC synthesis

Several exploratory and control syntheses were performed to optimize the conditions for the seeded synthesis of the Co/iron oxide nanocrystal heterojunctions. Thermal decomposition of $Co_2(CO)_8$ in mixtures that contained the TPs and surfactants (OLAC) did not lead to any heterogeneous Co deposition onto the seeds (already at low OLAC:Fe molar ratios), but yielded nearly spherical separate Co NCs (**Figure S5**). On the other hand, accomplishing the entire synthesis in the complete absence of surfactants led to poorly soluble network aggregates of Co-decorated TPs (**Figure S6**). Taken together, these observations suggested that relatively high concentration of OLAC could be used both to quench heterogeneous nucleation at any desired reaction stage and to ensure stabilization of the HNCs.

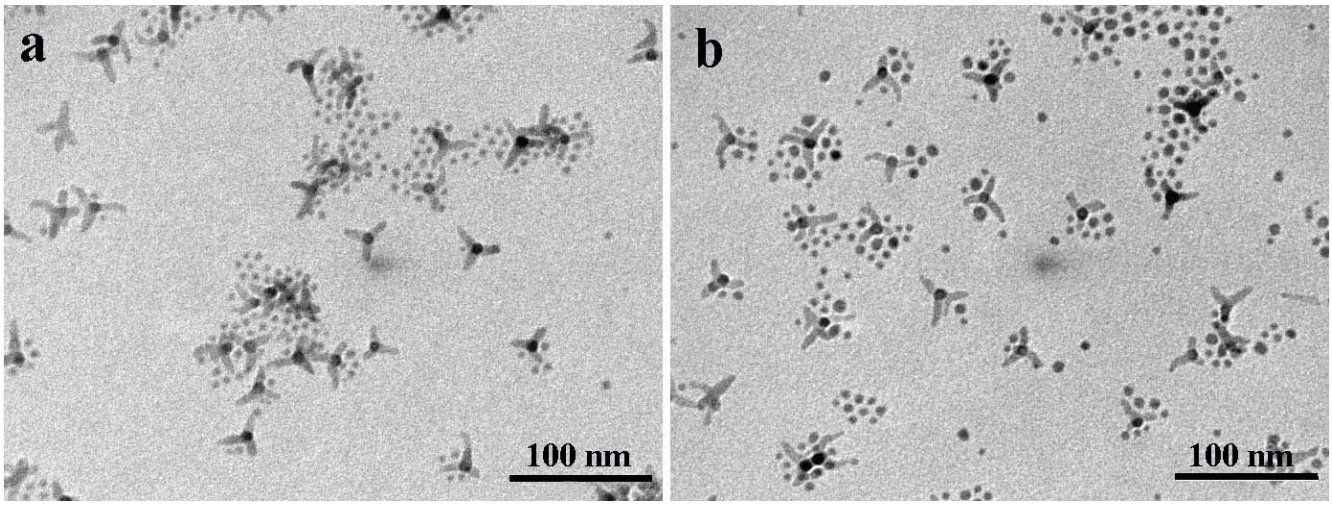

Figure S5: TEM images illustrating the nucleation of separate Co NCs upon decomposition of $Co_2(CO)_8$ in OLAC:TP seed mixtures. The initial iron oxide seed concentration (expressed in Fe units) was 0.04 M, while the Co:Fe:OLAC reactant molar ratio was set at 1:0.6:0.3 (**a**) and 1:0.6:0.1 (**b**), respectively.

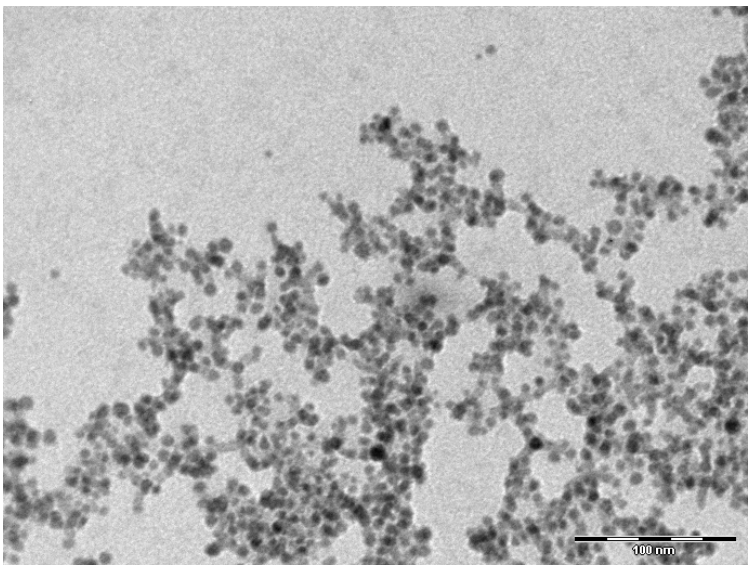

Figure S6 TEM images illustrating the tendency of the HNCs to form insoluble network aggregates upon decomposition of $Co_2(CO)_8$ in TP seed mixtures without performing any OLAC addition.

7. Magnetic measurements on HNCs carrying Co domains with different sizes

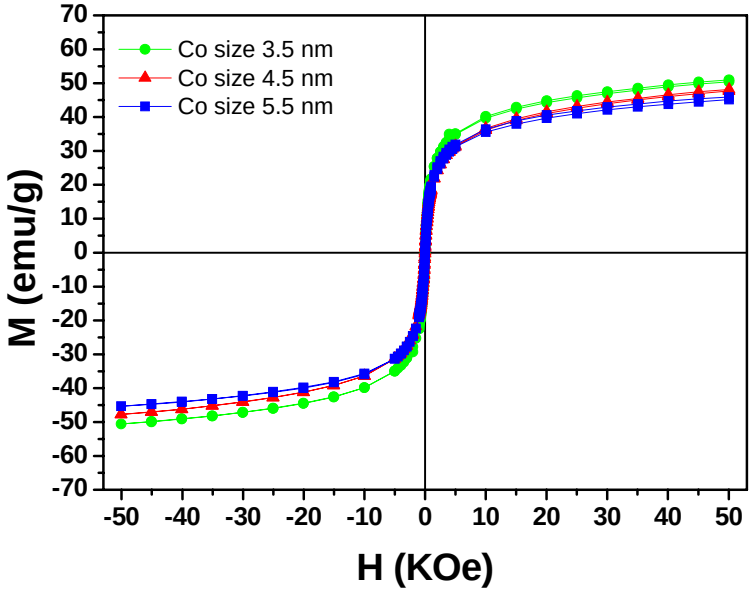

Figure S7 Magnetization curves recorded at 300 K for HNCs made of iron oxide TPs (with mean arm diameter and length sizes of 5±0.6 nm and 18±2 nm, respectively) decorated with Co domains of different mean sizes: 3.5 nm (green); 4.5 nm (blue); 5.5 nm (red), respectively

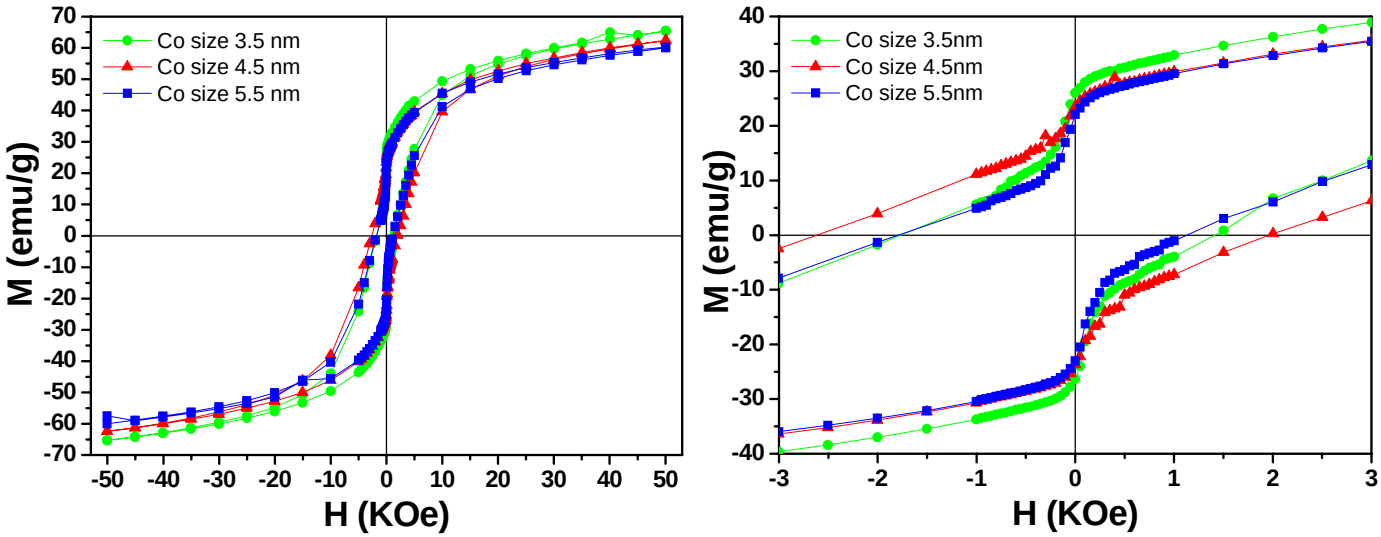

Figure S8 (Left panel) Full-view and (right panel) low-field expanded view of the magnetization curves recorded at 5K after ZFC for HNCs made of iron oxide tetrapods (with mean arm diameter and length sizes of 5±0.6 nm and 18±2 nm, respectively) decorated with Co domains of different mean sizes: 3.5 nm (green); 4.5 nm (blue); 5.5 nm (red), respectively.

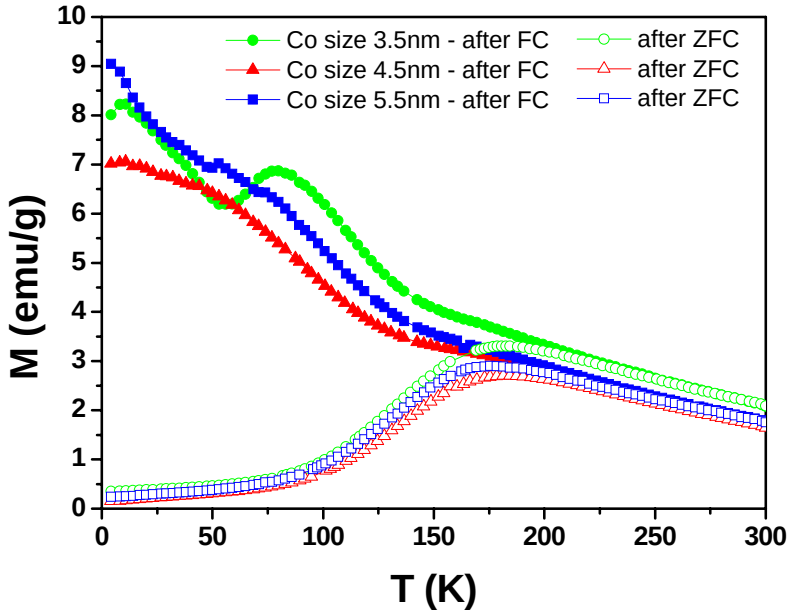

Figure S9 Temperature-dependent magnetization measurements under an applied field of 50 Oe after zero-field cooling (ZFC) and field-cooling (FC) with 5 T, of Co-decorated iron oxide tetrapods (with mean arm diameter and length sizes of 5±0.6 nm and 18±2 nm, respectively) carrying Co domains with different mean sizes: 3.5 nm; 4.5 nm; 5.5 nm, respectively

8. Determination of H_C and H_{EB} in the hysteresis curves

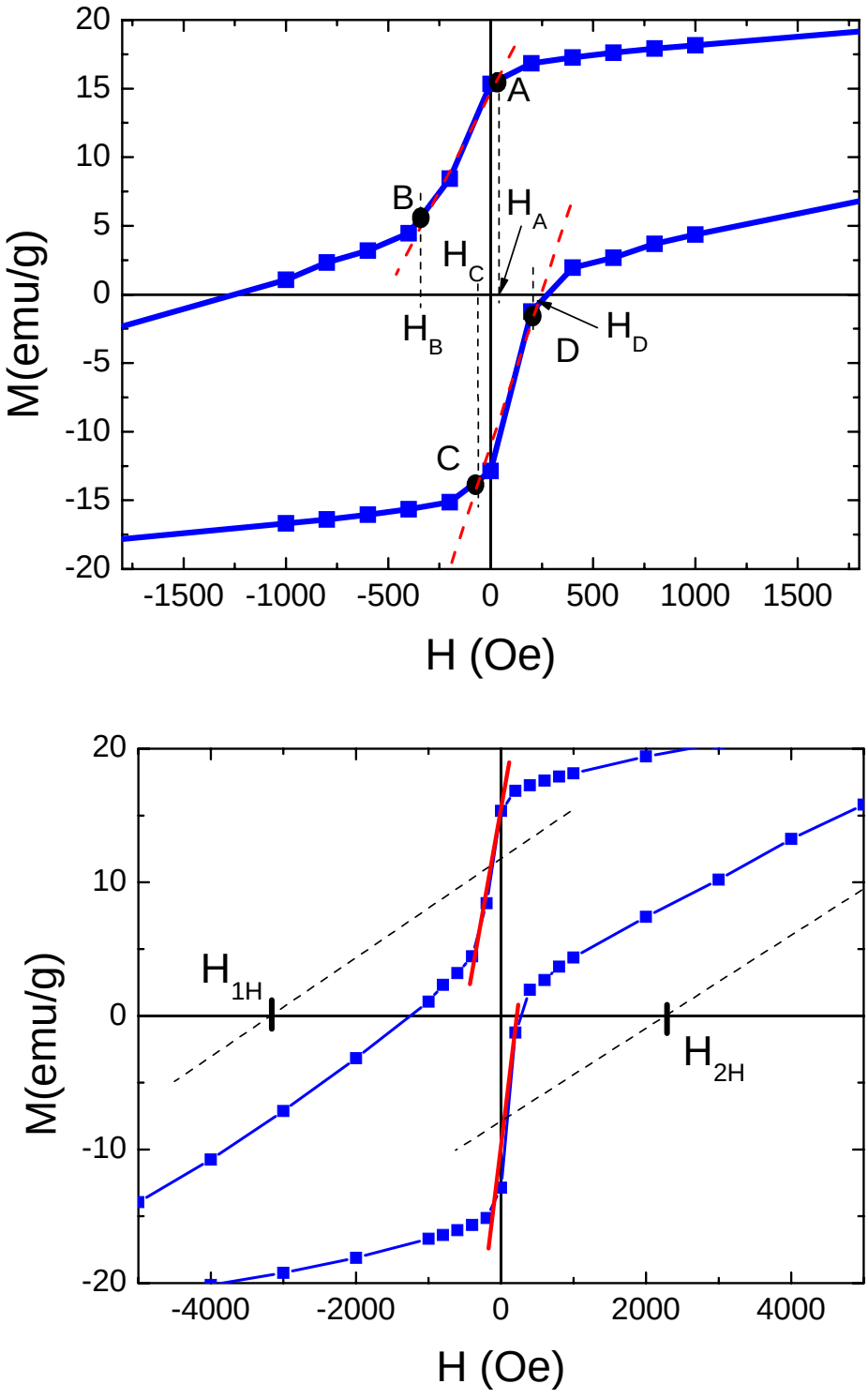

Figure S10 The figure illustrates the graphical procedure followed to estimate the H_C and H_{EB} values relative to the soft and hard phase components, respectively, in double-loop hysteresis curves. For sake of clarity, we have applied the procedure to the loop reported in Figure 4e of the main manuscript.

***Top panel - Estimation of the parameters for the soft phase*:** On the upper branch of the magnetization curve, we determine graphically the point at which the soft phase starts (point A) and

finishes (point B) to flip the magnetization, with the help of the visible red straight lines. On the basis of the H values corresponding to those points (i.e, H_A and H_B, respectively), we estimate the coercive field, H_{1S}, corresponding to the soft phase in this branch as the median value: $H_{1S}=(H_A+H_B)/2$. Analogously, we define the coercive field H_{2S} for the soft phase in the lower branch as: $H_{2S}=(H_C+H_D)/2$. Finally, the overall coercive field of the soft value, H_{CS}, and the related exchange bias shift along the field axis, H_{ES}, can be calculated from these values as follows:

$$H_{CS}=(H_{2S}-H_{1S})/2$$
$$H_{ES}=(H_{2S}+H_{1S})/2.$$

***Bottom panel - Estimation of the parameters for the hard phase*:** We draw straight lines parallel to the magnetization curve at the medium point of the section where the soft phase flips the magnetization (i.e., where it intersects the curve at H_{1S} and H_{2S}), at which the contribution of the soft phase is about zero. The points at which such straight lines intersect the horizontal axis (i.e, H_{1C} and H_{2C}) are approximately those where the curve should intercept the axis in the absence of the soft phase. The coercive field, H_{CH}, and the exchange bias shift, H_{EH}, relative to the hard phase, are calculated from these values as shown previously for the case of the soft phase:

$$H_{CH}=(H_{2H}-H_{1H})/2$$
$$H_{EH}=(H_{2H}+H_{1H})/2$$

References

[1] Cozzoli, P. D.; Snoeck, E.; Garcia, M. A.; Giannini, C.; Guagliardi, A.; Cervellino, A.; Gozzo, F.; Hernando, A.; Achterhold, K.; Ciobanu, N.; Parak, F. G.; Cingolani, R.; Manna, L., Colloidal Synthesis and Characterization of Tetrapod-Shaped Magnetic Nanocrystals. *Nano Lett.* **2006**, 6, (9), 1966-1972.

[2] Hammersley, A. P.; Svensson, S. O.; Hanfland, M.; Fitch, A. N.; Hausermann, D., Two-dimensional detector software: From real detector to idealised image or two-theta scan. *High Pressure Research* **1996**, 14, (4-6), 235-248.

[3] Altomare, A.; Burla, M. C.; Giacovazzo, C.; Guagliardi, A.; Moliterni, A. G. G.; Polidori, G.; Rizzi, R., Quanto: a Rietveld program for quantitative phase analysis of polycrystalline mixtures. *Journal of Applied Crystallography* **2001**, 34, 392-397.